J Solid State Electrochem (2007) 11:1191–1204
DOI 10.1007/s10008-006-0259-z

ORIGINAL PAPER

# Formulation of a holistic model for the kinetics of steady state growth of porous anodic alumina films

**G. Patermarakis · J. Chandrinos · K. Masavetas**

Received: 11 October 2006 / Revised: 10 December 2006 / Accepted: 19 December 2006 / Published online: 23 January 2007


**Abstract** A holistic model for the kinetics of steady state growth of porous anodic alumina films in oxalic acid, $H_2C_2O_4$, solution was developed not necessarily requiring the adoption of any 'a priori' mechanism of porous film growth. By this model the effect of anodising conditions on the transport numbers of $Al^{3+}$ cations and $O^{2-}$ anions across the barrier layer was revealed. The cation (anion) transport number decreased (increased) with current density, increased (decreased) with temperature and was unaffected by the concentration of electrolyte or pH. A complementary atomistic-ionic kinetic model was developed that fully justified these results and showed that the activation distances of $Al^{3+}$ and $O^{2-}$ transport are comparable, but the activation energy of $Al^{3+}$ transport is lower mainly due to the much smaller size of $Al^{3+}$. The validity of the model was tested on the basis of SEM observations, while structural features and the rate of pore wall dissolution were determined.

**Keywords** Al anodising · Porous anodic films · Steady state · Holistic kinetic model · Solid state ionic transport

## Introduction

Porous anodic alumina films are important materials applied to improve the mechanical properties of Al [1], as anticorrosion [2–4] and decorating [2, 3] coatings and membranes [5], in magnetic memories [6], catalysis [7–10], nuclear reactors [11], rechargeable batteries [12], as templates for synthesising emitters [13, 14], fuel cells [15] and the like. Due to the nanometer scale porous structure [2, 3, 7–10] and sizes of particles constituting the pore walls [16], they also found application in nanoscience and nanotechnology, e.g. forms for electroplating metal nanowires [17–19], templates for creating C [20, 21] or $TiO_2$ [22, 23] nanotubes, nanoparticle-sized ultra active catalysts or supports [7–10] and the like. Their optimal effectiveness depends on the suitable design of porous structure, nature/composition of pore wall oxide and reactive properties. They form in phosphoric, oxalic, chromic, sulphuric acid (and other sulphate) solutions [2, 3, 24–26], malonic, tartaric, citric and other acid solutions [27–29]. The structure of films is defined by the surface density, base diameter and shape of pores and their ordering degree.

The pore-forming anodising of Al is characterised by two transient stages followed by a steady-state one, AB, BC and CD in Fig. 1, for both galvanostatic and potentiostatic anodising. In the first stage, a flat barrier layer forms on the surface of which pores are later nucleated toward its end. In the second stage, pores are developed and self-organized yielding the characteristic hexagonal columnar cellular porous structure. Pores can nucleate and grow only under certain conditions [30]. The barrier type anodic alumina films grow by migration of $Al^{3+}$ ions outward and $O^{2-}$ ions inward [30, 31], with respective transport numbers $t_c$ and $t_a$ ($t_c+t_a=1$). For growth at 100% efficiency, about $t_c$ portion of the film thickness forms at the film/electrolyte interface due to migration of $Al^{3+}$ ions, the remainder forming at the metal electrolyte interface by migration of $O^{2-}$.

The growth of porous film occurs when no film material is added at the film/electrolyte interface, which corresponds to an efficiency of roughly 60% at conditions close, e.g., to current density 5 mA $cm^{-2}$, phosphoric acid concentration

G. Patermarakis (✉) · J. Chandrinos · K. Masavetas
School of Chemical Engineering,
Department of Materials Science and Engineering,
National Technical University,
Iroon Polytechniou 9, Zografou,
157 80 Athens, Greece
e-mail: gpaterma@central.ntua.gr

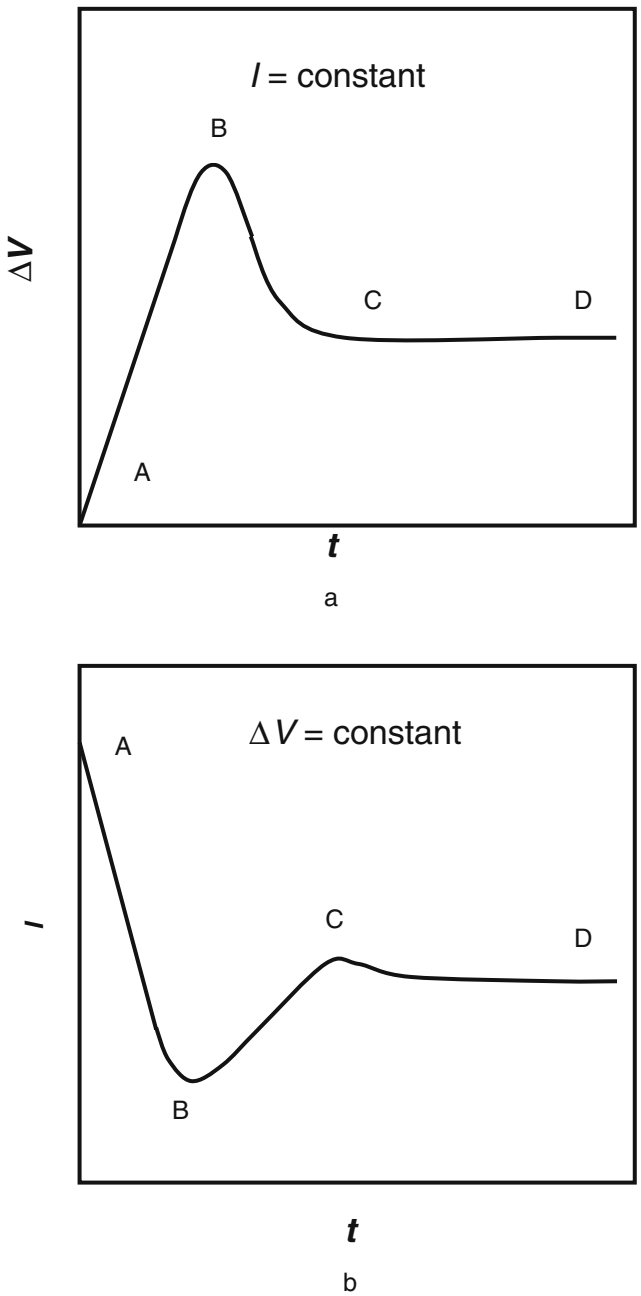


**Fig. 1** Variation of the anodising voltage, $\Delta V$, (or anodic potential) at constant current, $I$ (**a**) and of the anodising current, $I$, at constant voltage, $\Delta V$, (or anodic potential) (**b**) with time, $t$

0.4 M and temperature 20 °C [32, 33]. A flat film/electrolyte interface is then unstable in local perturbations of the electric field that can stabilize embryo pores. Pore filling is prevented by the absence of growth of new oxide at the film surface, while increased stresses from electrorestriction assist stabilization of the pores.

Pore generation is usually attributed to a thermally assisted, field-accelerated dissolution of oxide at the base of each pore [34]. The above model has been recently criticized [33] and another one, based on the plastic deformation of oxide in the barrier layer by the strong electrorestriction stresses, has been introduced. But irrespective of the adopted model, the formation of oxide occurs at the metal/oxide interface due to inward migration of $O^{2-}$ ions across the barrier layer [35, 36]. Simultaneously, $Al^{3+}$ ions migrate outward and are ejected to the electrolyte at the pore base. The $O^{2-}$ and $Al^{3+}$ contribute also roughly 60 and 40% of the ionic current in the barrier layer for anodising, e.g. in sulphuric acid at constant anodising voltage and temperature 14 °C.

In the steady state the interface Al/barrier layer oxide, consisting of close-packed hemispherical surface cavities, and pores base surface advance towards the Al side at equal rates yielding a porous layer consisting of about hexagonal columnar cells each of which contains an elongated pore normal to the surface and extending to the barrier layer. Its study is highly important as thick porous film with the extraordinary hexagonal cellular structure and elongated pores like parallel channels is developed exactly at this stage. The ionic transport inside the barrier layer below the porous layer of films has been studied to a small extent, opposite to flat barrier films, due to difficulties arising from the existence of porous layer above the scalloped barrier one. Oversimplifications for determining the $Al^{3+}$ and $O^{2-}$ transport numbers are frequently thus adopted, e.g. concerning them as the fractions of the cross-section surfaces of the average pore and pore wall oxide around pore bases, etc, that yields a rough only estimation. Also, it is hardly believed that they do not depend on the anodising conditions.

Thus, essentially, queries remain unanswered like the effect of the anodising conditions on the transport numbers and details of the ions transport mechanism. On the other hand, a holistic model capable of describing simultaneously the kinetics of ionic migrations in the barrier layer and the overall kinetics of growth of porous layer and its structural features in the steady state is absent. In this work, such a holistic model was formulated that, combined with chronopotentiometry and SEM, was used for studying the growth of porous anodic films. As the oxalic acid films are relatively pure materials with small amounts of electrolyte anions embodied in pore walls [24, 30] and usually with well-organised pores [37], oxalic acid electrolyte was used here.

## Experimental

Oxalic acid, $H_2C_2O_4$, solutions at concentrations ($C_{a,0}$)=0.5, 1 and 1.5 M were employed for Al anodising. Bath temperatures ($T$)=20, 25, 30 and 40 °C were employed for the first concentration, 25 °C for the second and 25 °C for the third where the solution was just saturated and 35 °C where it was unsaturated. Current densities ($j$)=5, 15 and 25 mA $cm^{-2}$ were employed at different times ($t$) up to

120 min. The pH of solutions, Table 1, was measured before and after each experimental run that showed no changes or minor ones.

Al sheets with thickness 0.5 mm and purity >99.5% were used. The remainder was Fe and Si in amounts <0.26 and 0.2% and traces of other elements. The shape and dimensions of the Al anodes and Pb cathodes used, the anodising procedure and the procedure for washing and neutralising Al anodes after anodising to remove the pore filling solution and contained compounds and drying were described earlier [38].

Al anodising was followed chronopotentiometrically. During anodising, the anodic potential, determined as previously [39], almost coincides with the potential drop from the oxide/electrolyte (o/e) interface to metal/oxide (m/o) interface [25] and is close to the anodising voltage. For convenience the latter was recorded. The voltage rise continued up to ≈90 V; then, anodising was interrupted, as higher voltages could cause a substantial rise of temperature in oxide bulk [40] notably exceeding that of bulk solution, thus prohibiting a strict control of conditions. The application of $j$>25 mA cm$^{-2}$ was practically impossible as the anodising voltage exceeded 90 V (e.g. at 25 °C) very early so that the acquisition of satisfactory kinetic data within a sufficiently long time interval was impossible. Anodes and cathodes were observed during anodising to reveal probable unusual phenomena. The structure of the oxide surface and the imprint of oxide on the Al substrate metal, revealed after the removal of the oxide by chromophosphoric acid solution [3, 38], was examined by SEM.

## Results and discussion

### General observations for the processes in anode and cathode

$H_2$ evolution on cathode ($2H^+ + 2e^- \rightarrow H_2$) did not occur within a long time interval from the start of anodising but later, at high anodising $t$'s, $H_2$ was evolved at a rate increasing with $j$ (and probably with $t$) and decreasing with $T$ and $C_{a,0}$. The absence of $H_2$ evolution or its slow rate (compared, e.g., to that in sulphate baths [38]) is due to cathodic electroreduction of $H_2C_2O_4$ occurring on high-hydrogen-overvoltage metals like Pb [41–43] that yields glyoxylic and glycolic acids and glyoxal. Thus, the effectivity of $H_2C_2O_4$ reduction increases with $T$ and $C_{a,0}$ and also varies with $j$ with an unsolved manner.

The $H_2C_2O_4$ solution films were yellowish more at high $t$'s. Such a colouration never occurred, e.g. in sulphate solutions films [25, 38]. It may be due to products of $H_2C_2O_4$ reduction embodied in the barrier layer and pore walls, like glyoxal that is yellow [44]. But equally well the yellowish colouration may be due also to the embodied electrolyte anions and derivative species [29] responsible for colour centres in the lattice, etc. As verified, the mass of consumed Al in the steady state, i.e. the difference of the initial mass of Al specimen and that after the removal of the oxide film by chromophosphoric acid solution [3, 38], accurately obeys Faraday's law. In Al anodes the $Al^{3+}$ ions entering the bath solution form aluminium oxalate. The amount of acid transformed in both anode and cathode, assuming even 100% efficiency, was negligible compared to the amount of acid in the bath solution that is consistent with the observed negligible pH change (≈0); thus, the acid concentration is essentially constant during the film growth.

### Chronopotentiometric study

The anodising voltage ($\Delta V$) vs $t$ plots appear in Fig. 2. Three stages were observed, in accordance with Fig. 1a. An initial transient stage appeared in which within a $t$ of the order of 10 s $\Delta V$ rises rapidly up to a maximum $\Delta V$ value ($\Delta V_M$) at $t=t(\Delta V_M)=t_M$. The $t_M$ and $\Delta V_M$ values depend on $T$, $C_{a,0}$ and $j$. Within the last range of this stage, the porous structure is nucleated [27, 28, 45, 46]. In the second

**Table 1** Values of parameters $t_a$, $z_1$, $z_2$ and correlation coefficient, COR, derived from fitting Eq. 14 to the experimental results and of parameter $t_{a,r}$ derived from this equation at $t=t_m$ for Al anodising in $H_2C_2O_4$ at different concentrations, $C_{a,0}$, temperatures, $T$, and current densities, $j$

| $C_{a,0}$/M | $T$ (°C) | $j$ (mA cm$^{-2}$) | pH | Parabolic model, Eq. 14 | | | | | Linear model ($z_2$=0) | | | |
|---|---|---|---|---|---|---|---|---|---|---|---|---|
| | | | | $t_a$ | $10^4 z_1$/min$^{-1}$ | $10^6 z_2$/min$^{-2}$ | COR | $t_{a,r}$ | $t_a$ | $10^4 z_1$/min$^{-1}$ | COR | $t_{a,r}$ |
| 0.5 | 20 | 15 | 0.701 | 0.7781 | −5.34 | 2 | 0.9689 | 0.7795 | 0.7725 | −2.94 | 0.9510 | 0.7733 |
| 0.5 | 25 | 15 | 0.728 | 0.7294 | −1.25 | −0.08 | 0.9652 | 0.7298 | 0.7296 | −1.35 | 0.9651 | 0.7299 |
| 0.5 | 30 | 15 | 0.695 | 0.7084 | −6.21 | 2.4 | 0.9950 | 0.7096 | 0.7035 | −3.35 | 0.9670 | 0.7041 |
| 0.5 | 40 | 15 | 0.705 | 0.6662 | −15.09 | −3.3 | 0.9985 | 0.6642 | 0.6728 | −18.95 | 0.9968 | 0.6703 |
| 0.5 | 25 | 5 | 0.728 | 0.6659 | −2.57 | −0.00023 | 0.9898 | 0.6648 | 0.6659 | −2.57 | 0.9898 | 0.6648 |
| 0.5 | 25 | 25 | 0.728 | 0.7569 | −0.358 | −1.4 | 0.3451 | 0.7570 | 0.7571 | −0.749 | 0.3428 | 0.7573 |
| 1 | 25 | 15 | 0.488 | 0.7326 | −2.99 | 0.147 | 0.9985 | 0.7330 | 0.7324 | −2.82 | 0.9984 | 0.7327 |
| 1.5 | 25 | 15 | 0.442 | 0.7439 | −7.91 | 4.16 | 0.9838 | 0.7415 | 0.7401 | −4.62 | 0.9692 | 0.7387 |
| 1.5 | 35 | 15 | 0.417 | 0.6820 | −5.76 | −10.4 | 0.9969 | 0.6832 | 0.6927 | −14.1 | 0.9861 | 0.6955 |

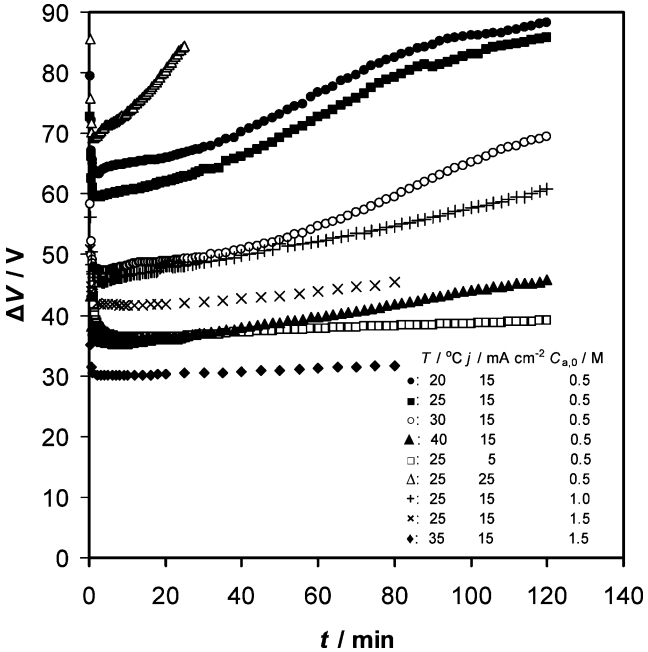


**Fig. 2** Variation of the anodising voltage, $\Delta V$, with time, $t$, at different temperatures, $T$, current densities, $j$, and electrolyte concentrations, $C_{a,0}$

transient stage $\Delta V$ drops and becomes minimum $\Delta V_m$ at a time $t(\Delta V_m)=t_m$ of the order of 1 min.

During this transient stage, the pore/cell system units develop and cover gradually all the surface and are self-organised to a more regular ordering within each metal grain surface or in the whole surface [47–54], the proper almost final number of cells/pores is set up and a quasi-steady-state pore-base diameter, nature/composition of barrier layer and electrolyte composition in pores is finally achieved. In the last, quasi-steady state, stage $\Delta V$ generally increases with $t$. All $\Delta V_M$, $\Delta V_m$ and the rate of $\Delta V$ rise with $t$ ($t>t_m$) increase with $j$ and decrease with $T$ and $C_{a,0}$. The $t_m$ shows a tendency to decrease with $j$ and increase with $T$ and $C_{a,0}$. The rise of $\Delta V$ with $t$ in the steady state cannot be ascribed to the main metal impurities due to their low percentage and much lower formation enthalpy of their oxides than that of alumina [55]; thus their atoms are not accumulated in the m/o interface [30], which could yield a noticeable $\Delta V$ rise during this stage. Much purer Al (>99.95%) showed a quite similar behaviour postulating the above suggestion.

## SEM observations and determination of basic structural features at certain case conditions

Metallographic specimens were prepared from the anodized Al specimens and the cross-sections of films were observed by SEM, as shown in Fig. 3. The thicknesses of $H_2C_2O_4$ films ($h$) thus measured vs $t$ ($\geq t_m$) plots at $C_{a,0}$=1.5 M, $j$=15 mA cm$^{-2}$ and $T$=25 and 35 °C are given in Fig. 4.

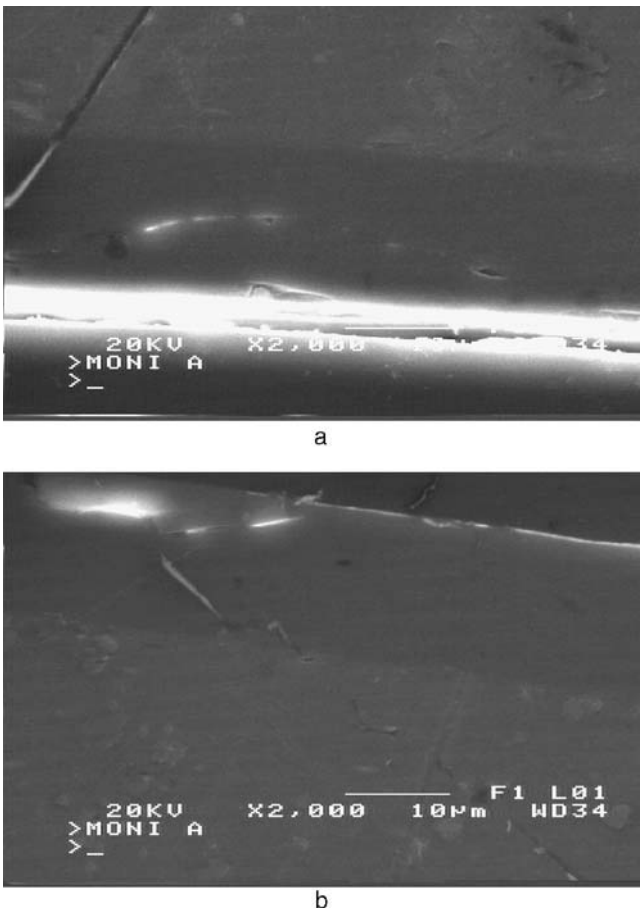


**Fig. 3** SEM photomicrographs showing the thickness of anodic film in two cases at $j$=15 mA cm$^{-2}$, $C_{a,0}$=1.5 M, $t$=40 min and $T$=25 °C (**a**) and 35 °C (**b**)

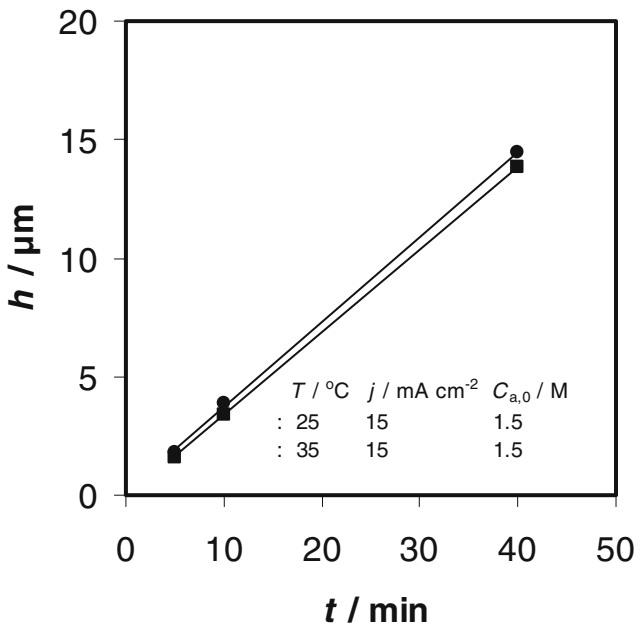


**Fig. 4** Variation of film thickness, $h$, with time, $t$, at $j$=15 mA cm$^{-2}$, $C_{a,0}$=1.5 M and $T$=25 and 35 °C

Linear dependences are observed with inclinations $k'$=0.358 and 0.349 μm $min^{-1}$, intersections close to 0 and correlation coefficients COR=0.9996 and 0.9999. It seems that $k'$ slightly decreases with $T$.

SEM micrographs of the surfaces of films at $T$=25 °C, $t$'s $\geq t_m$ and $C_{a,0}$=1.5 M (highest $C_{a,0}$, thus electrolyte is more aggressive; widening of pores at film surface with $t$ is larger and pores are better observed) and of the metal surface after removing the film by chromophosphoric acid solution, are shown in Figs. 5 and 6.

The film surface, Fig. 5a,b, shows pores that are irregularly spread, narrow, of rather irregular shape and slightly enlarged with $t$, as expected, due to the generally low chemical dissolution effect of electrolyte. There is no any explicit order of pores, Fig. 5a. Also, some protrusions (bright entities) are spread on the surface surrounded by pores near their boundaries as clearly shown in Fig. 5b. As observed, the surface density of these protrusions decreases and their average size increases with $t$ and both generally vary with the conditions. These protrusions, with size comparable to cell width (see below), must be involved in the mechanism of pore nucleation the study of which is, however, beyond the scope of this work.

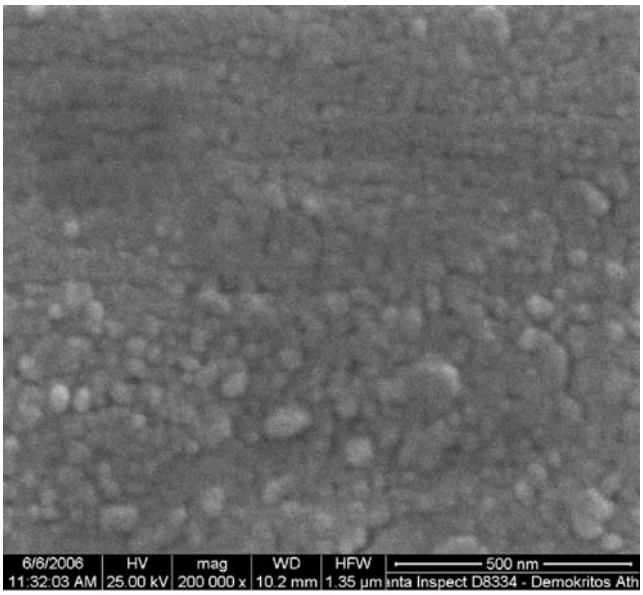


**Fig. 5** SEM photomicrographs of the structure of film surfaces at $j$=15 mA $cm^{-2}$, $C_{a,0}$=1.5 M, $T$=25 °C and $t$=5 min (**a**) and 40 min (**b**)

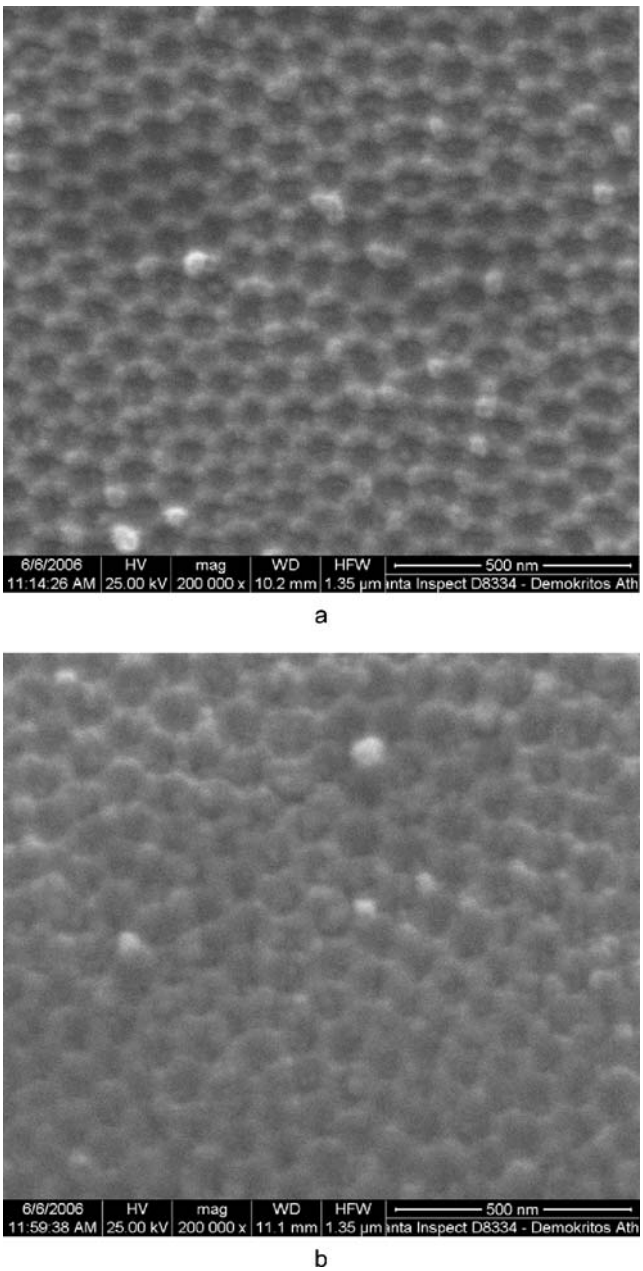


**Fig. 6** SEM photomicrographs of the imprints of anodic film on the Al surface at $j$=15 mA $cm^{-2}$, $C_{a,0}$=1.5 M, $T$=25 °C and $t$=5 min (**a**) and 40 min (**b**)

The Al substrate surface in Fig. 6 shows ordered imprints of cells, at $t$'s near $t_m$ locally approaching perfect hexagonal ordering that is disturbed for larger regions, (Fig. 6a). The pores/cells appear at arbitrary sites on the surface (see Fig. 5), but soon a self-ordering mechanism is put forward organizing the cells/pores up to $t_m$ (Fig. 6a). The hexagonal ordering is better for $t$'s $\geq t_m$ but near $t_m$ (Fig. 6a) than at higher enough $t$'s (Fig. 6b). Ordering and disordering processes must coexist, where ordering predominates at $t \leq t_m$ and disordering at $t > t_m$. While ordering spontaneously advances at $t > t_m$ (as at $t \leq t_m$), for inherent (e.g. mechanical) reasons of self-ordering mechanism, simultaneously, probably the variation of the resistance of pore-filling electrolyte at distinct surface positions results in a slow, gradual decay of uniformity of current passage and thus of pores/cells ordering. This resistance increases with pore length and is affected by the average pore diameter, composition of pore-filling solution and local hydrodynamic and mass/charge and heat transport conditions, while its relative changes are enlarged with pore length. Thus, the best ordering occurs at specific low thickness for each condition, near $h(t_m)$.

Small protrusions and hollow crests are regularly arranged in the boundaries of each triad and dyad of neighbouring hemispherical cavities as a result of close-packed arrangement. Protrusions of larger size also appear in sites where the ordering became disturbed in different ways. Most probably the processes in the pore above each protrusion are retarded for reasons given above, and within a short time interval, yielding the growth of Al protrusion under the corresponding cell/pore unit. The local current through the neighbouring cell/pore units instantly rises, accelerating these processes and increasing the thickness of the barrier layer. In turn, its increase retards the processes, and thus a more or less uniform advance of m/o interface occurs; simultaneously, the expansion of lateral cells soon leads to digestion of Al protrusion and to new local cell/pore system units arrangement, e.g. not hexagonally ordered. But this mechanism can similarly produce ordering elsewhere on the surface.

The cell size is almost independent of $t$ or $h$ ($t \geq t_m$), depending primarily on $j$ [56]. From Fig. 6 it is estimated to be $D_c \approx 99.4$ nm. As for organized pores $nD_c^2 = 4/3$ [39], where $n$ is the surface density of pores, then $n = 1.35 \times 10^{10}$ cm$^{-2}$, which is comparable to values found elsewhere [57–59]; the non-strict ordering along the whole surface does not create any problem, as there is interest mainly for the order of $n$ magnitude.

## The processes in the m/o and o/e interfaces and inside the barrier layer during the steady-state film growth

Before formulating the holistic model, a brief description of the processes in the barrier layer and m/o and o/e interfaces is cited to assist its conception. The material layer near the m/o interface is pure oxide and $Al^{3+}$ and $O^{2-}$ only migrate [24, 29, 30, 60–62] (Fig. 7). The valences of anions migrating in the barrier layer of films, growing, e.g. in sulphate solutions, are generally −1 and −2 [39] and in the remaining sublayer up to the o/e interface almost solely $O^{2-}$ and $OH^-$ anions move to the m/o interface (see also below). Al is consumed according to Faraday's law as shown here and earlier [38] and oxide forms in the m/o interface [39, 63] at a rate (mol/time) $J_{ox} = t_a j S_g (6F_c)^{-1}$. The rate of $Al^{3+}$ entering the m/o interface from the Al side is $jS_g(3F_c)^{-1}$, that of $Al^{3+}$ forming oxide is $t_a jS_g(3F_c)^{-1}$ and that of $Al^{3+}$ migrating to the o/e interface is $t_c jS_g(3F_c)^{-1}$ which, for constant $k'$ (as in the steady state), equals the rate of $Al^{3+}$ ejection to the solution at pore bases. The needed $O^{2-}$ for Al oxidation in the m/o interface comes from oxide lattice $O^{2-}$ and $OH^-$ coming from the dissociative adsorption of $H_2O$ on the film surface [25].

Due to the low standard formation enthalpy ($\Delta H^0$) of $C_2O_4^{2-}$ in aqueous solutions −845.2 kJ mol$^{-1}$ [64] and their symmetry, the embodied anions are stable, not decaying, e.g. to $O^{2-}$, even under the high field strength of the order of $10^7$ V cm$^{-1}$ [2, 3, 25]. These can only partially be transformed to derivative species, e.g. monocarboxylate ions within the layer of their incorporation [29] affected by the high field. These large anions cannot migrate via lattice sites of amorphous or nanocrystalline material as $O^{2-}$ and $OH^-$ do; they can supposedly move only in the boundary spaces between particles constituting the sublayer adjacent to the o/e interface [8, 16] negligibly contributing to the charge transfer. Such large spaces were also suggested to explain the incorporation of electrolyte anions [29, 61]. The verified movement of oxalate tracer ions during the growth of barrier type oxide toward the m/o interface at a rate much lower than that of $O^{-2}$ [65] is thus satisfactorily explained. As electrolyte anions are incorporated in a subalyer adjacent to the film surface, leaving a pure oxide sublayer adjacent to the m/o interface [24, 29, 30, 60–62], they do not contribute to the Al oxidation in the m/o interface.

The migration of $O^{2-}$ and of $OH^-$ inside the barrier layer, e.g. in a sublayer adjacent to the surface, at comparable rates, is possible because although the ionic radius of $O^{2-}$, 1.32 Å [44], is higher than that of $OH^-$, ≈0.96 Å [66], its charge is also higher. The enthalpy of $OH^-$ formation is not low enough, e.g. in aqueous solution $\Delta H^0 = -229.7$ kJ mol$^{-1}$ [64], and $OH^-$ can gradually decompose under the high-strength field, while moving inside the barrier layer where all $OH^-$ have decomposed up to the boundary of pure oxide layer. The product $O^{2-}$ migrate towards the m/o interface and $H^+$ towards the o/e interface where they are rejected in the solution at pore bases [39]. The existence of hydrogen species in small amount in compact oxide has been shown earlier [16, 38, 67].

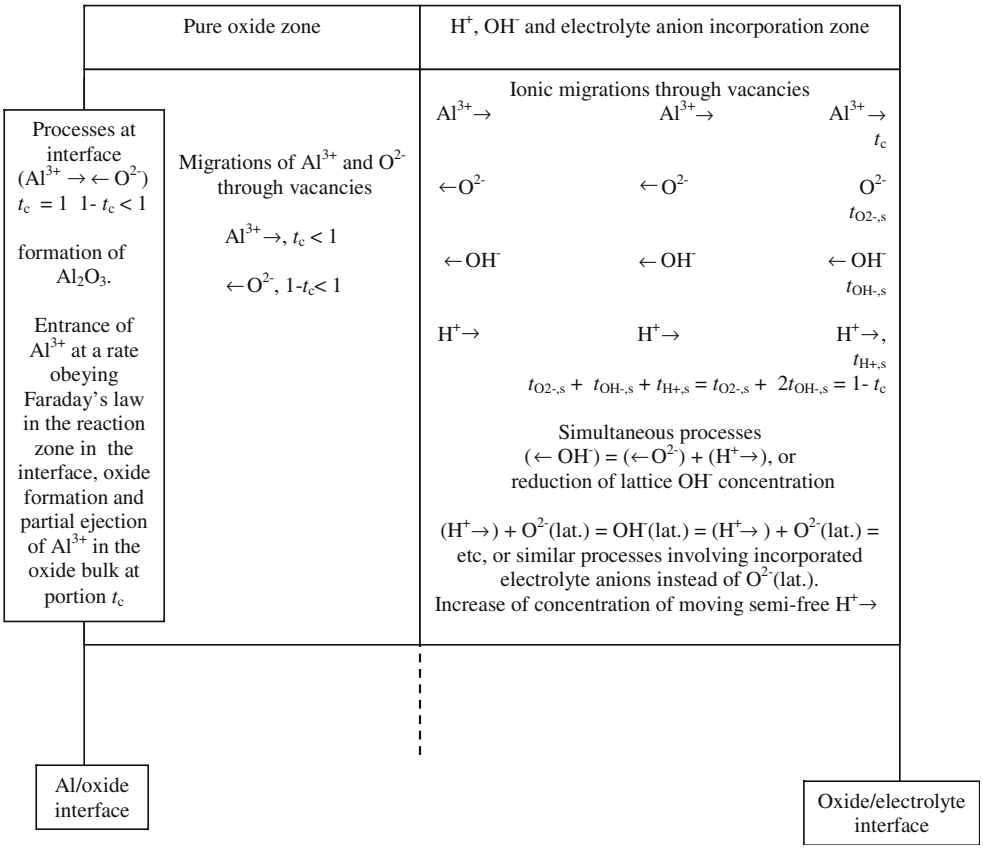


**Fig. 7** The ionic migrations inside the barrier layer. Two layers are distinguished, that adjacent to the metal where $O^{2-}$ and $Al^{3+}$ only migrate and the outer layer where additionally $OH^-$ and $H^+$ also migrate and electrolyte anions are embodied

Thus, excluding the pure oxide layer adjacent to the m/o interface, the ionic current inside the film is due to the migration of $O^2$, $OH^-$ and $H^+$ besides that of $Al^{3+}$. The flux rates (mol/time) of $O^{2-}$, $OH^-$, $H^+$ and $Al^{3+}$, $J_{O2-}$, $J_{OH-}$, $J_{H+}$ and $J_{Al3+}$, inside the layer adjacent to the o/e interface at each $t$ obey the charge transfer equations

$$2J_{O2-} + J_{OH-} + J_{H+} = jS_gF_c^{-1}(1 - t_c), \quad 3J_{A13+} = jS_gF_c^{-1}t_c \tag{1}$$

which at the surface become

$$2J_{O2-,s} + J_{OH-,s} + J_{H+,s} = 2J_{O2-,s} + 2J_{OH-,s} = jS_gF_c^{-1}(1 - t_c),\ 3J_{A13+,s} = jS_gF_c^{-1}t_c \tag{2}$$

The $J_{O2-}$ rises while both $J_{OH-}$ and $J_{H+}$ drop to the m/o interface; the latter become zero in the boundary of pure oxide sublayer where $2J_{O2-,m/o} = t_a jS_gF_c^{-1}2$. At the surface, $J_{O2-,s}$, $J_{OH-,s}$ and $J_{H+,s}$ acquire certain values depending on the conditions. The $J_{OH-}$ and $J_{H+}$ must drop strongly towards the m/o interface so that only a thin surface sublayer is highly enriched with these ions; thus the average concentration of H atoms in the barrier layer is actually small enough. For the more contaminated with anions $H_2SO_4$ films [2, 3, 24], the amount of contained $H_2O$ was found <0.5–1% *w*/*w* or at a portion <0.029–0.057% mol $H_2O$/mol $Al_2O_3$ [38]. The relevant amount of $H_2O$ and H atoms may be even lower in $H_2C_2O_4$ films as it may follow the amount of embodied anions.

## Development of a holistic model to a form determining the $Al^{3+}$ and $O^{2-}$ transport numbers in steady state

A kinetic model is developed under the conditions: (1) Not necessary requirement of the experimental determination of parameters like $k'$, $D_c$, pore base diameter ($D_b$), and density of compact pore wall oxide ($d_c$), and (2) without adopting 'a priori' any specific model for the mechanism of porous layer growth met in the literature [33, 34]. These are desirable for reasons explained below. It is only supposed that $n$ and the average $D_b$ remain constant in the steady state; as it will be seen later, this does not damage the general case of $D_b$ variation.

In the steady state of film growth ($t > t_m$), the film can be divided into three successive sublayers, Fig. 8a: (1) The scalloped barrier layer, consisting of hemispherical shell units, as those shown in the bottom of Fig. 8b, with cells/pores organised as possible is allowed by the material and conditions of anodising, at least locally within discrete regions, which are large compared to the average cell size [68]; it has mass $m_{bl}$ and height (Fig. 8b) $h_{bl}$; (2) an external

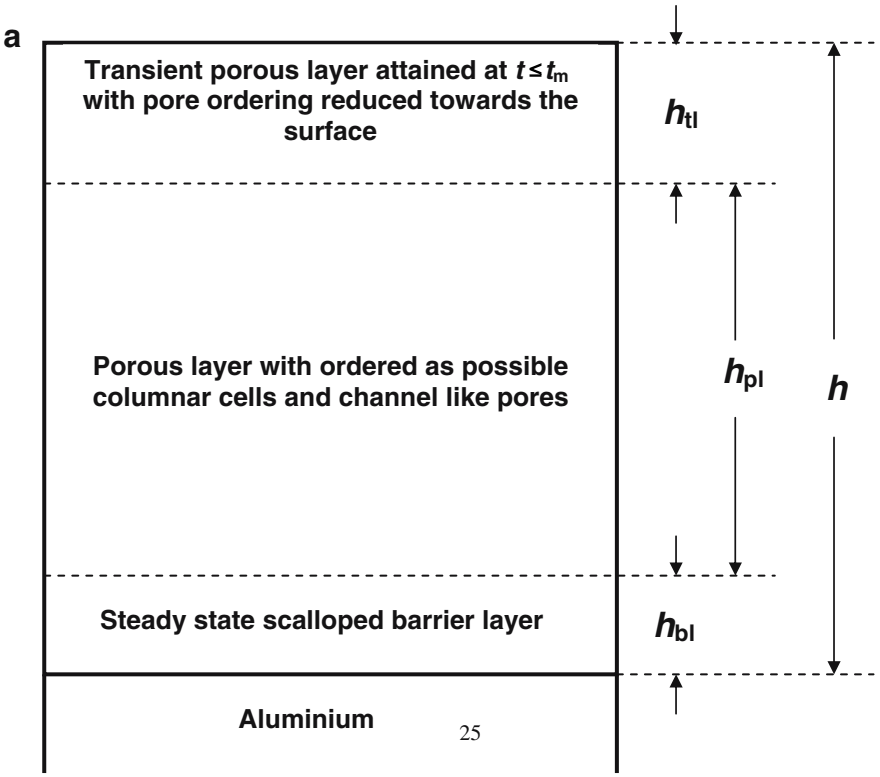


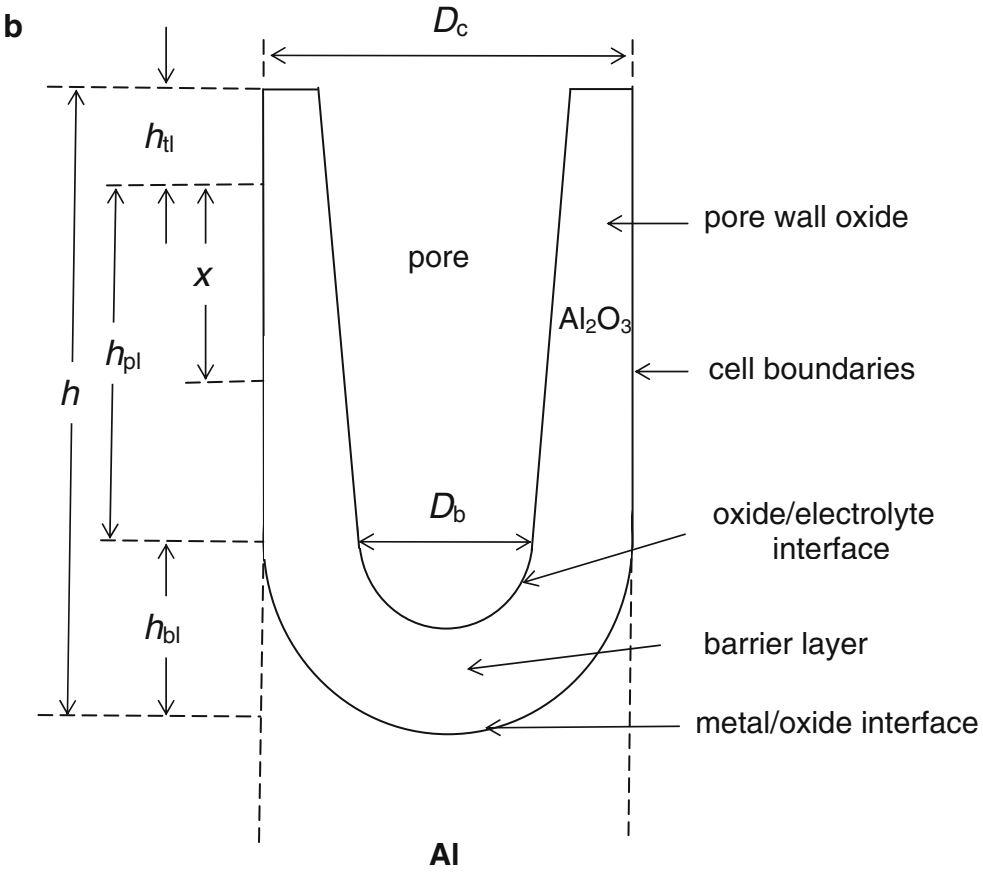


**Fig. 8** **a** The three successive layers of film in the steady state, the scalloped barrier layer with ordered pores and thickness $h_{bl}$, the porous layer with ordered pores and thickness $h_{pl}$ and the external porous transient layer without pore ordering towards the film surface and thickness $h_{tl}$. **b** Section parallel to pore axis of an ideal elongated, columnar cell of porous anodic alumina film. The pore, the pore base diameter, $D_b$, the cell size, $D_c$, the pore wall oxide, the hemispherical shell shaped barrier layer, the metal/oxide interface, the cell boundaries and the oxide/electrolyte interface are shown. The pore generally broadens towards the film surface as a result of pore wall chemical dissolution reaction by the electrolyte inside the pores and to some probable decrease of $D_b$ during the film growth

thin porous layer, developed up to $t=t_m$, with non-organised pores toward the surface and better organised toward its bottom that becomes the external layer at $t>t_m$ and has mass $m_{tl}$ and thickness $h_{tl}$; (3) the porous layer formed at $t>t_m$ lying between these layers, with organised pores, similar as the barrier layer units, and mass $m_{pl}$ and thickness $h_{pl}$. Thus, the mass of oxide ($m$) spread over the entire anodised Al specimen surface ($S_g$=30.75 cm$^2$ [38]) and its thickness at $t>t_m$ are given from equations

$$m = m_{bl} + m_{tl} + m_{pl} \tag{3}$$

$$h = h_{bl} + h_{tl} + h_{pl} \tag{4}$$

This $m$ in the steady state ($t>t_m$) (determined e.g. by film dissolution in chromophosphoric acid solution [3, 38]) is given also by the equation

$$m = m_0 + m_{mb} = m_0 + m_f - m_i + (AM_{Al})jtS_g(3F_c)^{-1}, \tag{5}$$

where $m_0$ is the mass of the initially present native passive layer and $m_{mb}$ is the mass added during anodising that is found by mass balance [69], $m_i$ is the initial mass of specimen, $m_f$ is the final mass of specimen after anodising, washing and drying, $(AM_{Al})jtS_g(3F_c)^{-1}$ is the mass of consumed Al according to Faraday's law, $F_c$ is Faraday's constant and $AM_{Al}$ is the atomic mass of Al. As the native passive layer has a thickness of the order of 1 or 10 nm [2, 3], $m_0$ is negligible compared to the $m$ values obtained at $t\geq t_m$, Fig. 9. Thus to a good enough approach

$$m = m_{mb} = m_f - m_i + (AM_{Al})jtS_g(3F_c)^{-1}(t\geq t_m) \tag{6}$$

The dependence of $m$ thus found on $t$ at different conditions is shown in Fig. 9.

The pores in the porous layer are slightly enlarged towards the film surface as a result of pore wall dissolution. This also occurs in the external thin layer. The decrease of its mass is negligible (→0) compared to $m$ at low $t$'s due to the slow pore wall dissolution; thus, the sum of the mass of barrier layer and external layer at low $t$'s essentially equals $m(t_m)$. Even at high $t$'s the amount of dissolved oxide in this layer is trivial compared to the mass of much thicker porous layer and thus its mass can be considered almost constant, that at $t_m$. The decrease of film thickness by dissolution at the used $t$'s is generally negligible compared to the thickness of film at $t=t_m$ [38]. The thickness of the external layer thus remains almost constant. Hence, both $m_{b1}+m_{t1}=m-m_{pl}$ and $h_{bl}+h_{tl}=h-h_{pl}$ can be considered constant for $t>t_m$ and equal to $m(t_m)$ and $h(t_m)$.

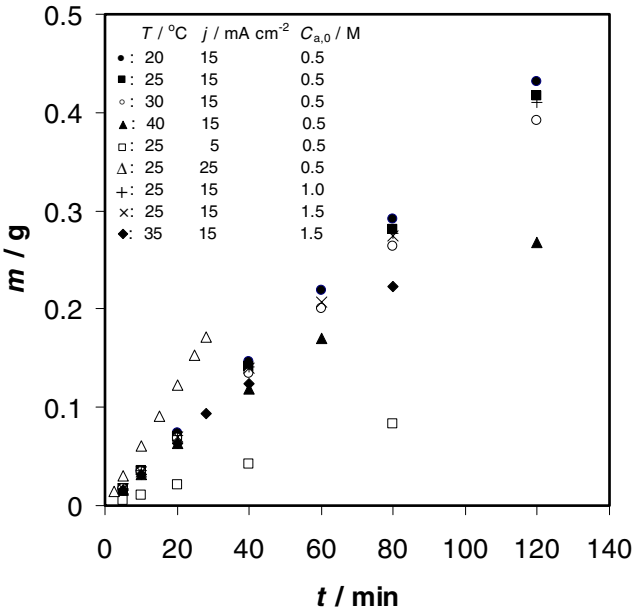


**Fig. 9** Variation of the film mass, $m$, with time, $t$, at different current densities, $j$, temperatures, $T$, and electrolyte concentrations, $C_{a,0}$

From Fig. 4 it is inferred that $h_{pl}$ is given by the equation

$$h_{pl} = k'(t - t_m) = k'\Delta t \tag{7}$$

where $k'$ generally depends on the anodizing conditions.

The $m_{pl}$ is the mass of the film occupying the geometrical space of film minus the mass of oxide corresponding to the void volume of pores, that is

$$m_{pl} = S_g h_{pl} d_c - V_{pl} d_c, \tag{8}$$

where $V_{pl}$ is the space of pores inside this layer given by the equation [56, 69]

$$V_{pl} = 4^{-1}\pi n S_g \int_0^{h_{pl}} \left(D_b + 2\int_{x/k'}^{h/k'} r_d dt\right)^2 dx = 4^{-1}\pi n S_g \int_0^{k'(\Delta t)} \left(D_b + 2\int_x^{k'(\Delta t)} r_d k'^{-1} dh\right)^2 dx, \tag{9}$$

where $r_d$ is the rate of chemical pore wall dissolution. For constant $n$ and average $D_b$ then generally [38, 69]

$$V_{pl} = 4^{-1}\pi n D_b^2 S_g k'(\Delta t) + a r_d (\Delta t)^2 + b r_d^2 (\Delta t)^3 = 4^{-1}\pi n D_b^2 S_g h_{pl} + \alpha' r_d h_{pl}^2 + b' r_d^2 h_{pl}^3 \tag{10}$$

For conical pores, i.e. when $D_b$ is constant and the $r_d$ is also constant along the pores or across the pore wall oxide, $\alpha = 2^{-1}\pi n S_g D_b k'$, $b = 3^{-1}\pi n S_g k'$, $\alpha' = 2^{-1}\pi n S_g D_b k'^{-1}$ and $b' = 3^{-1}\pi n S_g k'^{-2}$.

Thus in the start of steady state, $h_p=0$, $m_{pl}=0$ and $m(t_m) = m_{bl}+m_{tl}$ and at each $t>t_m$

$$m_{pl} = m - m(t_m) = \Delta m = \left(S_g h_{pl} - V_{pl}\right) d_c = d_c\left[S_g k'(\Delta t) - 4^{-1}\pi n D_b^2 k' S_g(\Delta t) - \alpha r_d(\Delta t)^2 - b r_d^2(\Delta t)^3\right] \quad (11)$$

or

$$P' = (\Delta m/\Delta t)\left(d_c S_g k'\right)^{-1} = 1 - 4^{-1}\pi n D_b^2 - \left[\alpha r_d(\Delta t) + b r_d^2(\Delta t)^2\right] = 1 - p, \quad (12)$$

where $P'$ is a dimensionless factor and $p$ is the porosity ($v/v$).

The rate of oxide formation in the m/o interface (mass/time) in the steady state, that is transformed to porous layer, is identical to the rate of the increase of the mass of porous layer around pore bases or

$$t_a kj S_g = S_g k' d_c\left(1 - 4^{-1}\pi n D_b^2\right) \text{ or } t_a kj = k' d_c\left(1 - 4^{-1}\pi n D_b^2\right), \quad (13)$$

where $k$ is a constant resulting from Faraday's law ($1.76097\times10^{-4}$ g $C^{-1}$). It applies irrespective of any model of porous layer growth mechanism. Merger of Eqs. 12 and 13 gives

$$P = (\Delta m/\Delta t)\left(kjS_g\right)^{-1} = t_a - t_a\left(1 - 4^{-1}\pi n D_b^2\right)^{-1}\left[\alpha k'^{-1} S_g^{-1} r_d(\Delta t) + b\, k'^{-1} S_g^{-1} r_d^2(\Delta t)^2\right] = t_a + z_1(\Delta t) + z_2(\Delta t)^2 \quad (14)$$

where $P$ is a dimensionless factor, $z_1 = -t_a\left(1 - 4^{-1}\pi n D_b^2\right)^{-1}\alpha\, k'^{-1} S_g^{-1} r_d$ and $z_2 = -t_a\left(1 - 4^{-1}\pi n D_b^2\right)^{-1} b\, k'^{-1} S_g^{-1} r_d^2$ are parameters for the first- and second-order terms. Actually, even if $D_b$ varies slightly with $t$ (quasi-steady state) the relevant effects are embodied mainly in the two last terms, the first one remaining unaffected as it is the limit of $P$ for $t\rightarrow t_m$. These are valid especially when available experimental points are crowded in the region of low $t$'s.

Available data of $m$ exactly at $t=t_m$ are not necessary. Data starting from a $t$ near $t_m$ ($t_{m,e}$), preferably at $t>t_m$, e.g. $m_{m,e}$, are only necessary. Then, the above procedure is applied considering $\Delta m = m - m_{m,e}$ and $\Delta t = t - t_{m,e}$. Such $P$ vs $\Delta t$ plots are shown in Fig. 10; in agreement to Eq. 14, plots are declining functions of $\Delta t$.

The $t_a$, $z_1$, $z_2$ and COR, determined by regression analysis, are given in Table 1. The $z_1$ is always <0, while $z_2$ is either <0 or >0 with negligible $|z_2|$ value $\rightarrow$0. The values of the second-order term of Eq. 14 thus always lie in the range of experimental error; the fact that it may be either <0 or >0 is thus justified and is not attributed to some inconsistency of Eq. 14. A more accurate value of $t_a$ (or real $t_a$, $t_{a,r}$) was found from the derived relationships for

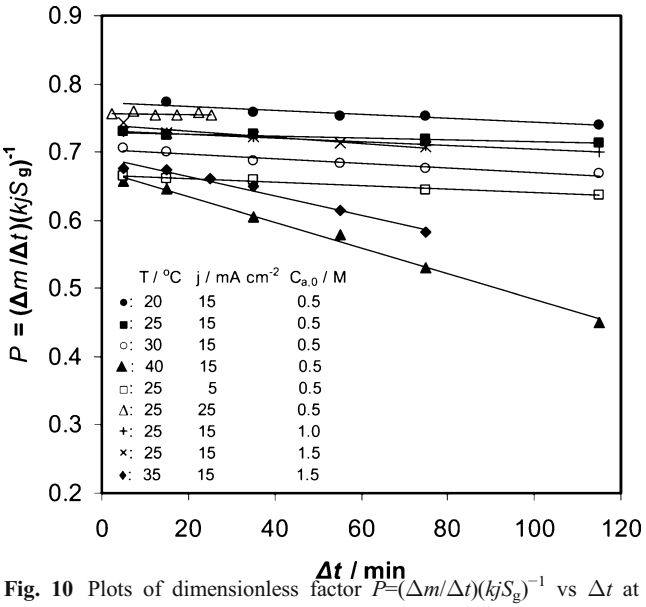


**Fig. 10** Plots of dimensionless factor $P=(\Delta m/\Delta t)(kjS_g)^{-1}$ vs $\Delta t$ at different current densities, $j$, temperatures, $T$, and electrolyte concentrations, $C_{a,0}$

$\Delta t=t_m-t_{m,e}$, Table 1, where $t_m$ was determined from the chronopotentiometric curves. However, $t_{a,r}$ and $t_{c,r}=1-t_{a,r}$ are close enough to $t_a$ and $t_c$, differing negligibly. For convenience, the linear plot ($z_2=0$), Fig. 10, was adopted; the relevant $t_a$, $z_1$, COR and $t_{a,r}$ are also cited in Table 1. It is noted that the COR value is always high, tending to 1, besides one only case, $j$=25 mA $cm^{-2}$, where the low value is attributed to the fact that the available experimental points are necessarily concentrated in narrow ranges along the $\Delta t$ and $P$ axes.

The $t_a$ ($t_c$) decreases (increases) with $T$, increases (decreases) with $j$ and is almost independent of $C_{a,0}$. The independence of $t_a$ and $t_c$ on $C_{a,0}$ shows that they indeed refer to the pure oxide layer adjacent to the m/o interface. The values of $t_a$ and $t_c$ at specific conditions, e.g. lower $j$'s and higher $T$'s approach those values met in the literature [32, 33], roughly 0.6 and 0.4, which, however, refer to other electrolytes. The $t_a$ and $t_c$ generally do not strongly vary with conditions; this may be the reason why the effect of conditions on them was not detected heretofore by the application of other experimental methods. Perhaps there is no other way to reach such calculations of $t_a$ and $t_c$ and to arrive at such conclusion with satisfactory accuracy. Any other way would need the application of different analytical methods of solid state to measure some or all the parameters $n$, $D_b$, $D_c$ (by SEM, TEM, AFM and similar methods), $h_{pl}$, $k'$ (by similar or other microscopic methods), $d_c$ (by similar methods, mass measurements methods), etc; usually an 'a priori' model for the mechanism of growth of porous layer, the real nature of which is actually under investigation, also should be adopted. Such an adoption will define 'a priori' to a large extent both the applied research method and

relevant results. The combination of various methods necessarily imparts errors degrading the accuracy of transport numbers determination; that is probably why these numbers determined by various other methods less precisely agree.

## Supplementary atomistic kinetic model for the ionic migrations in the region of scalloped barrier layer adjacent to the metal/oxide interface interpreting the dependence of transport numbers on the conditions

The elucidation of charge transport phenomena in the thin layer of oxide adjacent to the m/o interface, which is a pure oxide [24, 29, 30, 60–62], is highly important. The surface area of the m/o interface consisting of hemispherical surface units per $cm^2$ of $S_g$ is $S_c = 2^{-1}\pi n D_c^2$, which, as $nD_c^2$=4/3 [39], becomes $S_c$=2π/3=2.0944. The true partial ionic current densities across a hemispherical section surface adjacent and parallel to the m/o interface are thus $jt_aS_c^{-1}$ and $jt_cS_c^{-1}$. These must obey the high field strength Cabrera–Mott equation [70]

$$\begin{aligned} jt_aS_c^{-1} &= N_{2,m}\nu_2 n_2 F_c N^{-1}\exp\left[(W_2N + n_2a_2F_cE)/(RT)\right] \\ &= \lambda(3/5)]\nu_2 n_2 F_c N^{-1}\exp\left[(W_2N + n_2a_2F_cE)/(RT)\right] \\ &= Y\exp\left[(W_2\mathrm{N} + n_2a_2F_cE)/(RT)\right] \end{aligned} \quad (15)$$

$$\begin{aligned} jt_cS_c^{-1} &= N_{3,m}\nu_3 n_3 F_c N^{-1}\exp\left[(W_3N + n_3a_3F_cE)/(RT)\right] \\ &= \lambda(2/5)]\nu_3 n_3 F_c N^{-1}\exp\left[(W_3\mathrm{N} + n_3a_3F_cE)/(RT)\right] \\ &= Z\exp\left[(W_3N + n_3a_3F_cE)/(RT)\right], \end{aligned} \quad (16)$$

where $N_{2,m}$ is the surface concentration of mobile $O^{2-}$ that is proportional to 3/5 sites of the above section surface occupied by $O^{2-}$, $N_{2,m}$=λ(3/5), $N_{3,m}$ is the surface concentration of mobile $Al^{3+}$ that is proportional to the 2/5 sites occupied by $Al^{3+}$, $N_{3,m}$=λ(2/5), $\nu_2$ and $\nu_3$ are the vibration frequencies of ions, or the number of chances per second they may jump the energy barriers if they possess sufficient energies, $W_2$ and $W_3$ (<0) are the activation energies, $n_2$ and $n_3$ are the valences of ions, $a_2$ and $a_3$ are the activation (half-jump) distances, $N$ is the Avogadro constant, $R$ is the universal gas constant, $T$ is the temperature in K, $E$ (>0) is the field strength and $Y$ and $Z$ are constants with apparent meaning. Merger of Eqs. 15 and 16 for cancelling $E$ gives

$$\begin{aligned} &\ln\left[\left(jS_c^{-1}\right)^{[1/(n_2a_2)]-[1/(n_3a_3)]}\right] \\ &= \ln\left[(1-t_c)^{-[1/(n_2a_2)]}t_c^{[1/(n_3a_3)]}\right] + \ln\left[Y^{[1/(n_2a_2]}Z^{-[1/(n_3a_3)]}\right] \\ &\quad + [W_2/(n_2a_2) - W_3/(n_3a_3)]N/(RT) \end{aligned} \quad (17)$$

Investigation of Eq. 17 shows that

(1). If $1/(n_2a_2) - 1/(n_3a_3)>0$ (or when $a_2<(3/2)\ a_3$) then, when $j$ rises, $t_c$ always decreases, as observed (Table 1).

(2). As $1/(n_2a_2)>1/(n_3a_3)$, if $W_3>W_2$ or $|W_2|>|W_3|$ then $|W_2|/(n_2a_2) - |W_3|/(n_3a_3) >0$ or $W_2/(n_2a_2) - W_3/(n_3a_3) < 0$ and at constant $j$, on increasing $T$, $t_c$ necessarily increases, as observed (Table 1).

Because, as verified (Table 1) when $j$ and $T$ increase, the $t_c$ indeed, respectively, decreases and increases, then it appears that the activation distances are rather comparable for the ions $O^{2-}$ and $Al^{3+}$, as expected within the lattice of solid oxide, but the activation energy of $Al^{3+}$ transport (absolute value) is lower than that of $O^{2-}$. The latter is justified since, irrespective of the higher charge of cations, their much smaller size, ionic radius 0.51 Å, favours more their movement compared with the voluminous $O^{2-}$ with radius 1.32 Å [44].

From the corresponding $t_a$, $t_c$ and $j$ values, Table 1, both $jt_a$ and $jt_c$ increase with $j$. Then both Eqs. 15 and 16 show that $E$ (>0) increases with $j$, as expected, also verifying the above analysis.

## Application of the holistic model for determining other physical and structural features of films and kinetic parameters at certain case conditions. A test for the validity of model

As $nD_b^2>0$ then Eq. 13 shows that $d_c>t_akj/k'$ or $d_c>3.27$ and 3.16 g $cm^{-3}$ at $j$=15 mA $cm^2$, $C_{a,0}$=1.5 M and $T$=25 and 35 °C where the $k'$ values are available. These values are acceptable as $d_c$ should be lower than that of crystalline γ-$Al_2O_3$ 3.5–3.9 g $cm^{-3}$ [44] and close to values given earlier (3.0–3.42 g $cm^{-3}$ [3, 38, 61]). As $d_c$ is expected to differ trivially for the above two cases, then 3.27 g $cm^{-3}<d_c\leq$ 3.42 g $cm^{-3}$. Adopting a mean value $d_c$=3.345 g $cm^{-3}$ for both cases, then $nD_b^2$=0.0285 and 0.0974. From the $n$=$1.35\times10^{10}$ value at $T$=25 °C, $D_b$=14.52 nm. The anodising ratio is $2^{-1}(D_c-D_b)(\Delta V_m)^{-1}$=1.02 nm $V^{-1}$ and the average field strength $2(D_c - D_b)^{-1}(\Delta V_m)$ is $0.98\times10^7\approx10^7$ V $cm^{-1}$ that are acceptable [2, 3, 33, 62]. At $T$=35 °C considering $n$=$1.35\times10^{10}$ then $D_b$=22.94 nm. Because actually $n$ increases with $T$ [58, 59], then the real $D_b$ must be <22.94 nm and probably tends to become comparable to 14.52 nm [58, 59].

From the higher available $d_c$=3.42 g $cm^{-3}$, $nD_b^2$=0.0558 and 0.0974. Then in the first case $D_b$=20.03 nm, the anodizing ratio is 0.95 nm $V^{-1}$ and the average field strength is $1.05\times10^7\approx10^7$ V $cm^{-1}$. Considering $D_b\rightarrow0$, then an upper limit of anodising ratio exists that is 1.19 nm $V^{-1}$ with corresponding lower limit of field strength 0.84 V $cm^{-1}$. It is observed that the $D_b$ is very sensitive to $d_c$ variation. To accurately determine the $D_b$, $d_c$ must be

determined with high accuracy. The case $d_c$=3.345 g cm$^{-3}$ seems to approach better reality.

From the $t_a z_1$, $n$, $D_b$ and $nD_b^2$ values at $T$=25 °C $r_d$= 0.208 nm min$^{-1}$ ($nD_b^2$=0.0285) and 0.154 nm min$^{-1}$ ($nD_b^2$=0.0558). The increase of pore radius at film surface (see Fig. 5) is indeed comparable to the product of this value and the difference of corresponding $t$'s. These $r_d$'s almost equal 0.143 nm min$^{-1}$ [58] that, however, refers to higher $T$=40 °C but lower $C_{a,0}$=0.02 M.

### Interpretation of ΔV rise during the quasi-steady state and its dependence on anodising conditions

As shown, the process of ordering of columnar cellular porous structure practically ends at $t \approx t_m$ where the best ordering appears. The gradual weakening of ordering, e.g. at $T$=25 °C for $t > t_m$, is attained by a rise of $\Delta V$ (see Fig. 2), just as the progress of ordering with $t$ at $t_M \le t \le t_m$ is followed by its decrease. The variation of $\Delta V$ in the quasi-steady state is thus at least partially due to a reduction of ordering degree; this, however, needs a further research. But this can be partially ascribed also to a change of electrolyte composition in the pore base region.

$Al^{3+}$ are rejected in the pore filling solution mostly by the field caused $Al^{3+}$ ejection, and secondarily by the purely chemical dissolution of pore walls; thus, aluminium oxalate forms. The study of mass and charge transport phenomena in sulphate baths [71] showed that the concentration of salt always falls towards the mouths of pores, that of acid can either rise, fall or pass though a minimum at a position along the pores depending on the conditions and the contribution of anions to the charge transfer inside the pores is minor [72]. In $H_2C_2O_4$ the concentration of salt must also rise, but that of $H_2C_2O_4$ must fall towards the pore bases where it becomes $C_{a,b}$. As the contribution of anions to the charge transfer is minor, its drop must be due mainly to the faster consumption than pumping of $H_2C_2O_4$ molecules inside the narrow pores by the mass transfer driven by the gradient of concentration along the pores. For this reason and because of the effect of common anion of salt on the acid dissociation, the concentrations of free, not solvating $Al^{3+}$, electrolyte anions and $H^+$ also drop to the pore bases.

The $D_b$, besides $T$, also depends on $C_{a,b}$ and, e.g. for $H_2SO_4$ electrolyte, it increases with $C_{a,b}$ [25]. This must be valid also for $H_2C_2O_4$ baths. Then, $D_b$ must decrease and, because $D_c$ remains almost constant, $2^{-1}(D_c - D_b)$ increases, the average real $j$ increases and thus $\Delta V$ rises with $t$. This variation of electrolyte composition at pore bases with $t$, irrespective of the average cross-section surface of pore-filling electrolyte, is obviously enhanced with rising $j$, as $H_2C_2O_4$ is consumed at higher rate, and with falling $T$, unfavouring the mass transport of $H_2C_2O_4$ towards the pore bases, and is retarded with rising $C_{a,0}$, mainly because a larger amount of $H_2C_2O_4$ is available inside the pores; thus, the rise of $\Delta V$ with $t$ must be enhanced with increasing $j$ and decreasing $T$ and $C_{a,0}$ as exactly observed (Fig. 2). The elucidation of the part played by the gradual disordering with $t$ ($t > t_m$) and the change of electrolyte composition at pore bases with $t$ needs further investigation.

## Conclusions

1. A holistic model for the kinetics of growth of porous anodic alumina films in $H_2C_2O_4$ was developed by which the $Al^{3+}$ and $O^{2-}$ transport numbers inside the barrier layer in the steady state were determined in a large range of anodising conditions and their dependence on the conditions was theoretically successfully justified. The cation (anion) transport number decreases (increases) with $j$, increases (decreases) with $T$ and is unaffected by $C_{a,0}$ or pH and the saturated or unsaturated nature of pore-forming electrolyte. The activation distances of $Al^{3+}$ and $O^{2-}$ transport are comparable, but the activation energy of $Al^{3+}$ transport is lower than that of $O^{2-}$ mainly due to the much lower size of cations.
2. This model combined with chronopotentimetry and SEM observations predicted structural features of films and kinetic parameters of their growth validating its coherence.
3. The method may become a suitable tool to similarly discover the transport numbers during the first transient stage of flat barrier layer growth and in other pore-forming electrolytes and the effect of anodising conditions and electrolyte kind on them.
4. As the cation transport number determined here varies with current density and temperature similarly as the pore/cell surface density varies with these parameters [58, 59], the elucidation of the dependence of anions and cations transport number on the conditions and the mechanism of ions transport is expected to assist greatly the full elucidation of the real mechanism of pore nucleation.

Definitions of symbols

| | |
|---|---|
| $a$ | $2^{-1}\pi n S_g D_b k'$ |
| $a'$ | $2^{-1}\pi n S_g D_b k'^{-1}$ |
| $a_2$ | Activation (half-jump) distance for the migration of the $O^{2-}$ ions |
| $a_3$ | Activation (half-jump) distance for the migration of the $Al^{3+}$ ions |
| $AM_{Al}$ | Atomic mass of Al |
| $b$ | $3^{-1}\pi n S_g k'$ |
| $b'$ | $3^{-1}\pi n S_g k'^{-2}$ |

| | |
|---|---|
| $C_{a,0}$ | Concentration of $H_2C_2O_4$ in the bath bulk solution |
| $C_{a,b}$ | Concentration of $H_2C_2O_4$ in the pore base region |
| COR | Correlation coefficient |
| $d_c$ | Density of the compact pore wall oxide |
| $D_b$ | Pore base diameter |
| $D_c$ | Cell width |
| $\Delta V$ | Anodising voltage |
| $\Delta V_M$ | Maximum value of $\Delta V$ attained at the end of the first and start of the second transient stage of film growth |
| $\Delta V_m$ | Minimum value of $\Delta V$ attained at the end of the second transient stage and start of the quasi-steady state stage |
| $\Delta t$ | $t - t_{m,e}$ or $t-t_m$ |
| $\Delta m$ | $m-m_{m,e}$ or $m-m(t_m)$ |
| $E$ | Local field strength across the barrier layer |
| $F_c$ | Faraday's constant |
| $h$ | Total thickness of anodic film |
| $h_{tl}$, $h_{pl}$ and $h_{bl}$ | Thickness of transient layer and porous layer and height of barrier layer of the film |
| $I$ | Current |
| $j$ | Current density |
| $J_{OH-}$, $J_{O2-}$ and $J_{H+}$ | Local rates of migration of $OH^-$, $O^{2-}$ and $H^+$ inside the barrier layer oxide (mol/time) |
| $J_{OH-,s}$, $J_{O2-,s}$ and $J_{H+,s}$ | Rates of migration of $OH^-$, $O^{2-}$ and $H^+$ in the surface of barrier layer (mol/time). |
| $J_{O2-,m/o}$ | Rate of migration of $O^{2-}$ near the m/o interface (mol/time) |
| $J_{Al3+}$= $J_{Al3+,s}$ | Rate of migrating $Al^{3+}$ through the oxide towards the o/e interface and rejected to solution (mol/time) |
| $J_{ox}$ | $jt_aS_g(6F_c)^{-1}$ rate of oxide production in the m/o interface (mol/time) |
| $k$ | Rate constant for oxide production resulting from Faraday's law |
| $k'$ | Rate of film thickness growth |
| $\lambda$ | $N_{2,m}(3/5)^{-1} = N_{3,m}(2/5)^{-1}$= constant |
| $m$ | Mass of oxide film spread over the whole geometric surface area of Al specimens during anodising |
| $m_{fi}$ | Final (after anodising and drying) mass of the Al specimen |
| $m_{in}$ | Initial mass of the Al specimen |
| $m_0$ | Mass of the initial native passive layer on Al surface |
| $m_{mb}$ | Mass of oxide film added over the whole geometric surface area of Al specimens during anodising found by mass balance |
| $m_{tl}$, $m_{pl}$ and $m_{bl}$ | Mass of transient layer, porous layer and barrier layer of the film |
| $m_{m,e}$ | Film mass $m$ at the lower $t$ close to $t_m$ at which experimental results are available |
| m/o | Metal/oxide interface |
| $n$ | Surface density of pores in the quasi-steady state stage |
| $n_2$ | Valence of $O^{2-}$ |
| $n_3$ | Valence of $Al^{3+}$ |
| $N$ | Avogadro constant |
| $N_{2,m}$ | Surface concentration of mobile $O^{2-}$ ions |
| $N_{3,m}$ | Surface concentration of mobile $Al^{3+}$ ions |
| $\nu_2$ | Vibration frequency of $O^{2-}$, or the number of chances per second the ions may jump the energy barrier if they have sufficient energy |
| $\nu_3$ | Vibration frequency of $Al^{3+}$, or the number of chances per second the ions may jump the energy barrier if they have sufficient energy |
| o/e | oxide/electrolyte interface |
| $p$ | Porosity of the porous layer of the anodic film (volume/volume) |
| $P$ | $(\Delta m/\Delta t)(kjS_g)^{-1}$= dimensionless factor. |
| $P'$ | $(\Delta m/\Delta t)(d_cS_gk')^{-1}$ = dimensionless factor |
| $r_d$ | Rate of pore wall oxide dissolution reaction |
| $R$ | Universal gas constant |
| $S_g$ | Geometric surface area of Al specimens (30.75 $cm^2$) |
| $S_c$ | $2^{-1}\pi nD_c^2$ |
| $t$ | Anodising time |
| $t_a$ and $t_c$ | Transport number of $O^{2-}$ and $Al^{3+}$ inside the sublayer of barrier layer near the m/o interface consisting of pure oxide |
| $t_{a,r}$ and $t_{c,r}$ | More accurate, real, transport number of $O^{2-}$ and $Al^{3+}$ found by the $P(\Delta t)$ equation at $\Delta t=t-t_m$ |
| $t_M=t$ ($\Delta V_M$) | Time at the end of the first and the start of the second transient stage of film growth where the maximum $\Delta V$ is attained |
| $t_m=t$ ($\Delta V_m$) | Time at the end of the second transient stage and start of the quasi-steady state stage where the minimum $\Delta V$ is attained |
| $t_{m,e}$ | Lower $t$ close to $t_m$ at which experimental results are available |
| $V_{pl}$ | Void volume of the porous layer |
| $W_2$ | Height of the energy barrier (activation energy) for the migration of $O^{2-}$ ions |
| $W_3$ | Height of the energy barrier (activation energy) for the migration of $Al^{3+}$ ions |
| $x$ | Distance from the boundary of porous layer and transient layer along the pore axis |

| | |
|---|---|
| $Y$ | $\lambda(3/5)\nu_2 n_2 F_c N^{-1}$ |
| $Z$ | $\lambda(2/5)\nu_3 n_3 F_c N^{-1}$ |
| $z_1$ and $z_2$ | Parameters derived by fitting equation $P=t_a+z_1(\Delta t)+z_2(\Delta t)^2$ to the experimental results $P$ vs $\Delta t$ |

**Acknowledgements** Many thanks to Dr Chr. Chandrinou from the Institute of Materials Science, NCSR Demokritos, for her assistance with SEM.

## References


1. Leach SL, Neufeld F (1969) Corros Sci 9:225
2. Diggle JW, Downie TC, Goulding CW (1969) Chem Rev 69:365
3. Young L (1961) Anodic oxide films. Academic, London
4. Shreir LL (1976) Corrosion, vol. 2. Newnes-Butterworths, London
5. Smith AW (1973) J Electrochem Soc 120:1068
6. Kawai S, Ishiguro I (1976) J Electrochem Soc 123:1047
7. Ihm SK, Ruckenstein E (1978) IEC Prod Res Dev 17:110
8. Patermarakis G, Moussoutzanis K, Chandrinos J (1999) Appl Catal A Gen 180:345
9. Patermarakis G, Nikolopoulos N (1999) J Catal 187:311
10. Ganley JC, Riechmann KL, Seebauer EG (2004) J Catal 227 (1):26
11. Bai XD, Heming C, Ma CL, Peng DQ, Duo D, Zhong DX, Lu JF, Guo BH, Xin Z, Bai GM, Guo JL (2004) Rare Met Mater Eng 33:300
12. Mozalev A, Magaino S, Imai H (2001) Electrochim Acta 46:2825
13. Holland ER, Li Y, Abbott P, Wilshaw PR (2000) Displays 21:99
14. Gaponenko NV, Molcham IS, Thompson GE, Skeldon P, Pakes A, Kudrawiec R, Bryja L, Misiewicz J (2002) Sens Actuators A99:71
15. Bocchetta P, Chiavarotti G, Masi R, Sunseri C, Di Quarto F (2004) Electrochem Comm 6:923
16. Patermarakis G, Kerassovitou P (1992) Electrochim Acta 37:125
17. Zhang Z, Gekhtmann D, Dresselhaus M, Ying J (1999) Chem Mater 11:1659
18. Wang Z, Kuok M, Ng S, Fan H, Lockwood D, Nielsch K, Wehrspohn R (2001) Mater Phys Mech 4:22
19. Gao T, Meng G, Zhan J, Wan Y, Lian C, Fa J, Zhan L (2001) Appl Phys A 73:251
20. Li J, Papadopoulos C, Xu JM, Moskovits M (1999) Appl Phys Lett 75:367
21. Che G, Lakshmi B, Fisher E, Martin C (1998) Nature 393:346
22. Michailowski A, Almawlawi D, Cheng G, Moskovits M (2001) Chem Phys Lett 349:1
23. Gong D, Grimes C, Varghese O, Hu W, Singh R, Chen Z, Dickley D (2001) J Mater Res 16:3331
24. Thompson GE, Furneaux RC, Wood GC (1978) Corros Sci 18:481
25. Patermarakis G, Moussoutzanis K, Chandrinos J (2001) J Solid State Electrochem 6:39
26. Patermarakis G (2006) J Solid State Electrochem 10:211
27. Surganov VF, Gorokh GG (1993) Mater Lett 17:121
28. Surganov V, Janson C, Nielsen JCG, Morgen P, Gorokh G, Larsen AN (1988) Electrochim Acta 33:517
29. Yamamoto Y, Baba N (1983) Thin Solid Films 101:329
30. Thompson GE (1997) Thin Solid Films 297:192
31. Brown F, Mackintosh WD (1973) J Electrochem Soc 120:1096
32. Thompson GE, Xu Y, Skeldon P, Shimizu K, Han SH, Wood GC (1978) Phil Mag B55:651
33. Garcia-Vergara SJ, Skeldon P, Thompson GE, Habazaki H (2005) Electrochim Acta 52:681
34. Hoar TP, Mott NF (1959) J Phys Chem Solids 9:97
35. Siega J, Ortega C (1977) J Electrochem Soc 124:883
36. Cherki C, Siejka J (1973) J Electrochem Soc 120:784
37. Sui YC, Cui BZ, Martínez L, Perez R, Sellmyer DJ (2002) Thin Solid Films 406:64
38. Patermarakis G, Lenas P, Karavassilis Ch, Papayiannis G (1991) Electrochim Acta 36:709
39. Patermarakis G, Moussoutzanis K (1995) Electrochim Acta 40:699
40. Applewhite FR, Leach JSL, Neufeld P (1969) Corros Sci 9:305
41. Goodridge F, Lister K, Plimley RE, Scott K (1980) J Appl Electrochem 10:55
42. Tilak EV, Weinberg NL (1982) Technique of electroorganic synthesis, Part III. Wiley, New York
43. Zhou YL, Zhang XS, Dai YC, Yan WK (2003) Chem Eng Sci 58:1021
44. Weast RC (ed) (1980) Handbook of Chemistry and Physics, 60th (edn). CRC, Boca Raton, p B-52, C-323, F-214
45. Dell'Oca CJ, Fleming PJ (1976) J Electrochem Soc 123:1487
46. Parkhutik VP (1986) Corros Sci 26:295
47. Li AP, Müller F, Birner A, Nielsch K, Gösele U (1997) J Appl Phys 84(11):6023
48. Jessensky O, Müller F, Gösele U (1998) Appl Phys Lett 72 (10):1173
49. Zhang L, Cho HS, Li F, Metzger RM, Doyle WD (1998) J Mater Sci Lett 17:291
50. Jessensky O, Müller F, Gösele U (1998) J Electrochem Soc 145:3735
51. Li AP, Müller F, Gösele U (2000) Electrochem Solid State Lett 3 (3):131
52. Masuda H, Yotsuya M, Asano M, Nishio K, Nakao M, Yokoo A, Tamamura T (2001) Appl Phys Lett 78(6):826
53. Nielsch K, Choi J, Schwirn K, Wehrspohn RB, Gösele U (2002) Nano Letters 2(7):677
54. Pan H, Lin J, Feng Y, Gao H (2005) IEEE Transactions on Nanotechnology 3:462
55. Xu Y, Thompson GE, Wood GC, Bethune B (1987) Corros Sci 27:83
56. Patermarakis G, Moussoutzanis K (1995) J Electrochem Soc 142:737
57. Martin CR (1996) Chem Mater 8:1739
58. Nagayama M, Tamura K, Takahashi H (1970) Corros Sci 10:617
59. Takahashi H, Nagayama M (1978) Corros Sci 18:911
60. Takahashi H, Fujimoto K, Nagayama M (1988) J Electrochem Soc 135:1349
61. Thompson GE, Wood GC, Shimizu K (1981) Electrochim Acta 26:951
62. Xu Y, Thompson GE, Wood GC (1983) J Electrochem Soc 130:2395
63. Ono S, Ichinose H, Masuko N (1991) J Electrochem Soc 138:3705
64. Dodos D (1975) Electrochemical data. Elsevier, Budapest
65. Shimizu K, Habazaki H, Skeldon P, Thompson GE, Wood GC (2001) Electrochim Acta 46:4379
66. Sanderson RT (1976) Chemical bonds and bond energy, 2nd edn. Academic, New York
67. Lanford WA, Alwitt RS, Dyer CK (1980) J Electrochem Soc 127:405
68. Li AP, Müller F, Birner A, Nielsch K, Gösele U (1997) J Vac Sci Technol A17(4):1428
69. Patermarakis G, Tzouvelekis D (1994) Electrochim Acta 39:2419
70. Cabrera N, Mott NF (1948) Rep Prog Phys 12:163
71. Patermarakis G (1998) J Electroanal Chem 447:25
72. Patermarakis G (1996) J Electroanal Chem 404:69